

# Quantification of Human Central Adipose Tissue Depots: An Anatomically Matched Comparison Between DXA and MRI

Christopher D. Crabtree<sup>1</sup>, Richard A. LaFountain<sup>1</sup>, Parker N. Hyde<sup>1</sup>, Chong Chen<sup>2</sup>, Yue Pan<sup>3</sup>, Nathan Lamba<sup>2</sup>, Teryn N. Sapper<sup>1</sup>, Jay A. Short<sup>1</sup>, Madison L. Kackley<sup>1</sup>, Alex Buga<sup>1</sup>, Vincent J. Miller<sup>1</sup>, Debbie Scandling<sup>3</sup>, Irma Andersson<sup>4</sup>, Samantha Barker<sup>4</sup>, Houchun H. Hu<sup>5</sup>, Jeff S. Volek<sup>1</sup>, and Orlando P. Simonetti<sup>3,4,6</sup>

<sup>1</sup>Department of Human Sciences, <sup>2</sup>Department of Biomedical Engineering, <sup>3</sup>Dorothy M. Davis Heart & Lung Research Institute, and <sup>4</sup>Department of Radiology, The Ohio State University, Columbus, OH; <sup>5</sup>Department of Radiology, Nationwide Children's Hospital, Columbus, OH; and <sup>6</sup>Division of Cardiovascular Medicine, Department of Internal Medicine, The Ohio State University, Columbus, OH

## Corresponding Author:

Orlando P. Simonetti, PhD  
320 Biomedical Research Tower, 460 West 12<sup>th</sup> Ave,  
Columbus, OH 43210;  
E-mail: Simonetti.9@osu.edu

## Key Words:

MRI, DXA, visceral, adipose, metabolic syndrome  
**Abbreviations:** Visceral adipose tissue (VAT), subcutaneous adipose tissue (SAT), dual-energy X-ray absorptiometry (DXA), magnetic resonance imaging (MRI), metabolic syndrome (MetSyn), intra-abdominal adipose tissue (IAAT), body mass index (BMI), high-density lipoprotein (HDL), low-density lipoprotein (LDL), blood pressure (BP), Digital Imaging and Communications in Medicine (DICOM), fat percentage (FP), water percentage (WP), region of interest (ROI), hepatic portal vein (HPV), standard deviation (SD), nonalcoholic fatty liver disease (NAFLD)

## ABSTRACT

Excess visceral adipose tissue (VAT) and VAT volume relative to subcutaneous adipose tissue (SAT) are associated with elevated health risks. This study compares fat measurements by dual-energy X-ray absorptiometry (DXA) and magnetic resonance imaging (MRI). In total, 21 control subjects (Control) and 16 individuals with metabolic syndrome (MetSyn) were scanned by DXA and MRI. The region measured by MRI was matched to the android region defined by DXA, and MRI reproducibility was also evaluated. In addition, liver fat fraction was quantified via MRI and whole-body fat by DXA. VAT measurements are interchangeable between DXA and MRI in the Control ( $R = 0.946$ ), MetSyn ( $R = 0.968$ ), and combined cohort ( $R = 0.983$ ). VAT/SAT ratio did not differ in the Control group ( $P = .10$ ), but VAT/SAT ratio measured by DXA was significantly higher in the MetSyn group ( $P < .01$ ) and the combined ( $P = .03$ ) cohort. Intraobserver (ICC = 0.998) and interobserver (ICC = 0.977) reproducibility of MRI VAT measurements was excellent. Liver fat fraction by MRI was higher ( $P = .001$ ) in MetSyn ( $12.4\% \pm 7.6\%$ ) than in controls ( $2.6\% \pm 2.2\%$ ), as was whole-body fat percentage by DXA ( $P = .001$ ) between the MetSyn ( $42.0\% \pm 8.1\%$ ) and Control groups ( $26.7\% \pm 6.9\%$ ). DXA and MRI VAT are interchangeable when measured over an anatomically matched region of the abdomen, while SAT and VAT/SAT ratio differ between the 2 modalities.

## INTRODUCTION

The visceral adipose tissue (VAT) surrounding the abdominal organs contributes to central obesity and has been described as an inflammatory endocrine organ associated with negative health consequences (1, 2) including elevated risk for cardiovascular disease and diabetes (3). Subcutaneous adipose tissue (SAT) is not as strongly linked with metabolic disease (4); however, VAT/SAT ratio has been cited as a predictor of mortality and cardiac events independent of total VAT volume (5). The distribution of fat stored in the VAT, SAT, and specific organ depots such as the liver, has a prognostic value superior to surrogate measures such as body mass index (BMI) or waist circumference (2). It is therefore important to carefully consider the limitations and

differences between current methods used to measure VAT and SAT storage depots.

Dual-energy X-ray absorptiometry (DXA), X-ray computed tomography (CT), and magnetic resonance imaging (MRI) are currently used for the noninvasive estimation of visceral fat. DXA is increasingly utilized in healthcare and nonclinical settings because it is a rapid, easy-to-use, inexpensive option when compared with other modalities (6), and it accurately measures whole-body and visceral fat. DXA uses 2-dimensional projection data created by low energy, fan beam X-ray to create a model consisting of bone, adipose, and lean tissue compartments. VAT assessment via DXA

Crabtree and LaFountain are co-first authors.

has been previously validated (7), but it is important to note that DXA VAT measurements may be spatially limited. For example, the Lunar iDXA system running Automated CoreScan<sup>™</sup> software (GE, Madison, WI) estimates VAT from the iliac crest to 20% of the distance to the base of the skull by subtracting subcutaneous fat from total fat within that region (6, 8). A significant portion of the upper abdomen is thereby excluded (8, 9). VAT estimation by DXA is achieved by first detecting the thickness of SAT at the lateral periphery of the android region, and then applying an anthropometric model to estimate the total SAT compartment (9). SAT is then subtracted from total fat within that region to estimate VAT.

MRI has several advantages over DXA in quantification of abdominal fat (10) and is considered to be a reference standard (6). VAT quantification by MRI is not spatially restricted, enabling imaging and quantification of fat in the entire abdomen. MRI is a cross-sectional tomographic imaging modality that has the ability to precisely distinguish fat depots throughout the body. MRI does not use ionizing radiation and can quantify the fractional fat content of liver, skeletal muscle, heart, and other organs (11, 12).

Separation of fat depots into SAT and VAT alone may be an oversimplification, and MRI has the potential for differentiation of other abdominal fat depots. Fat within the abdomen and pelvis, excluding SAT, is more appropriately called intraabdominal adipose tissue (IAAT) (13, 14). True VAT is only 1 component of IAAT that strictly includes only fat within the peritoneal cavity, while excluding retroperitoneal fat and any fat within the abdominal muscle wall, spinal fat, and intraorgan fat (14). Retroperitoneal fat is of specific interest as it is exterior to the mesentery (15) and lacks portal classification (16), but it is impossible to distinguish by DXA.

Comparisons of DXA with MRI (7, 17, 18) have previously shown that their VAT measurements are highly correlated (2, 6, 7, 15). In addition, comparisons of DXA and MRI in which regions of interest (ROI) were anatomically matched (17, 19) have concluded that the modalities have a high level of agreement. SAT measurements by DXA and MRI conversely have not been as close in agreement (19). There are inherent strengths and weaknesses associated with each modality, and several factors including cost, availability, radiation exposure, scan duration, and ability to provide additional relevant clinical information may provide guidance for the application of one over the other. This study examines the relationship between DXA and MRI quantification of VAT, SAT, and VAT/SAT ratio in a cohort of subjects including patients meeting the criteria for metabolic syndrome (MetSyn), as well as a Control group. Together, these subjects cover a wide range of adiposity. Complementary parameters including whole-body fat content by DXA, liver fat fraction by MRI, and incidental findings on MRI were also evaluated to illustrate the potential value of additional information that can be provided by each instrument.

## METHODOLOGY

### Participant Characteristics

The study was approved by the local Biomedical Institutional Review Board, and written informed consent was obtained from all participants. Sixteen patients with MetSyn and 21 controls with no evidence of metabolic disease locally recruited for 2 independent diet intervention trials were used in this study. Baseline

DXA and MRI measurements were taken before any dietary interventions. Subject characteristics including demographics, anthropometrics (height, weight, BMI, and waist circumference), blood pressure, and blood biomarkers (glucose, total cholesterol, HDL, LDL, and triglycerides) are listed in Table 1.

A diagnosis of MetSyn was confirmed in all (n = 16) subjects in the MetSyn group based on the requirement (20) that at least 3 of the following 5 measures exceed categorical cut points: elevated waist circumference (>102 cm in men and >88 cm in women), elevated triglycerides ( $\geq 150$  mg/dL), reduced HDL-C (<40 mg/dL in men <50 mg/dL in women), elevated blood pressure (systolic BP  $\geq 135$  and diastolic BP  $\geq 85$ ), and elevated fasting glucose ( $\geq 100$  mg/dL) (20). Although no participants in the Control cohort (n = 21) were classified as having MetSyn, 4 subjects met 1 criteria, and 6 met 2 criteria.

### Dual-Energy X-Ray Absorptiometry

A single, whole-body DXA measurement was performed on each subject using a Lunar iDXA system. CoreScan<sup>™</sup> (GE, Lunar, enCORE software version 14.10) calculated VAT and SAT mass in addition to whole-body fat percentage.

### Magnetic Resonance Imaging

MetSyn patients were imaged on a 3 T scanner (MAGNETOM Tim Trio, Siemens Healthineers, Erlangen, Germany) and the controls on a 1.5 T scanner (MAGNETOM Avanto, Siemens Healthineers). The 2 cohorts were recruited for different research trials, and each trial used a different MRI scanner. Although this inconsistency should be noted, the technique used for fat quantification was identical on the 2 systems, and the results are not expected to be affected by field strength (21).

The VARiable PROjection (VARPRO) pulse sequence (22) was used in both cohorts to generate the in-phase, out-of-phase, water, water percentage, fat, and fat percentage images that were used to measure abdominal fat volumes (VAT and SAT) and liver fat fraction. The VARPRO pulse sequence is a rapid scan technique that acquires 3D volumetric images covering the entire abdominal region in a single breath-hold and automatically generates the images required for fat-water separation. The VARPRO pulse sequence parameters used in each cohort are listed in Table 2.

### Selection of MRI Slices for Comparison With DXA

Although the MRI scan covered a length of 300–360 mm of the abdomen, VAT and SAT were quantified only in a subset of the acquired slices anatomically matched to the region analyzed by the DXA Automated CoreScan<sup>™</sup> software. DXA calculated the fat distribution in the android region defined as 20% of the distance from the top of the iliac crests to the base of the skull (9). Anatomical matching between DXA and MRI was achieved by using the spinal vertebrae as a reference; the vertebrae are visible in both DXA and MRI images as seen in Figure 1. To match the anatomy used for analysis, first the coronal DXA projection was overlaid on the labeled coronal DXA vertebral X-ray image (Figure 1A). The positions of the upper and lower bounds of the android region automatically defined by the DXA software were noted with respect to the vertebrae (Figure 1A). These positions were then matched with the vertebrae visible in a sagittal MRI

**Table 1.** Participant Characteristics<sup>a</sup>

Demographics	MetSyn (n = 16)	Control (n = 21)	P
Sex	7 = ♀	4 = ♀	
	9 = ♂	17 = ♂	
Asian	n = 0	n = 3	
Black or African American	n = 1	n = 1	
Hispanic or Latino	n = 1	n = 1	
White	n = 14	n = 16	
Anthropometrics			
Height (cm)	174.1 ± 8.6	176.7 ± 6.91	.321
Weight (kg)	114.9 ± 17.8	85.6 ± 12.1	.001*
BMI (kg/m <sup>2</sup> )	38.1 ± 6.1	27.4 ± 3.3	.001*
Biometrics			
Systolic BP (mmHg)	128.9 ± 7.1	115.7 ± 9.1	.001*
Diastolic BP (mmHg)	83.8 ± 8.4	76.9 ± 7.7	.014*
Blood Glucose (mg/dL)	103.6 ± 9.2	90.4 ± 10.5	.001*
Fasting HDL (mg/dL)	Total = 37.3 ± 10.7	Total = 48.8 ± 13.2	
	♀ = 42.4 ± 11.0	♀ = 51.3 ± 14.5	.007*
	♂ = 33.3 ± 9.1	♂ = 49.5 ± 14.1	
Triglycerides (mg/dL)	178.4 ± 65.4	132.9 ± 95.4	.112
Waist Circumference (cm)	Total = 112.6 ± 15.7	Total = 94.9 ± 11.9	
	♀ = 104.3 ± 14.0	♀ = 93.3 ± 8.7	.001*
	♂ = 115.2 ± 14.3	♂ = 95.3 ± 12.7	

\*Statistical significance between groups, *P* < .05.

<sup>a</sup> Variables shown as Mean ± SD.

localizer image [Figure 1\(B\)](#) to select the MRI slices matching the region analyzed by DXA ([Figure 1C](#)). This allowed a direct comparison of the abdominal fat measurements by the 2 modalities within the android region defined by DXA ([Figure 1, D and E](#)). The selected ranges were then reviewed by a radiologist to confirm the accuracy. The MRI images acquired in the MetSyn cohort were also reviewed by a radiologist for incidental findings.

### Semiautomatic Segmentation of Visceral and Subcutaneous Adipose Tissue

The DICOM MRI images were processed using a semiautomated, custom-built application programmed in MATLAB (The MathWorks, Inc, Natick, MA). The application automatically segments and quantifies VAT and SAT compartment

volumes and includes tools for manual editing of the segmentation results. It should be noted that the algorithm does not specifically exclude spinal or retroperitoneal fat storage depots; these are included within VAT.

The following 4 image types were used during the segmentation process: fat percentage (FP), in-phase, water, and water percentage (WP). The semiautomated segmentation process comprised 4 steps as outlined in [Figure 2](#). First, in step 1 ([Figure 2A](#)), thresholds of FP ≥ 50% and WP ≤ 50% were applied to the FP and WP images, respectively, on a pixelwise basis to define a binary fat mask. Standard morphological operators included with the MATLAB Image Processing Toolbox were applied to the fat mask to remove the arms and background air and to fill all pixels within the outer boundaries of the fat mask, thus defining

**Table 2.** Magnetic Resonance Imaging Sequence Parameters

	Field Strength	TA	Total Slices	TR	TE	Flip Angle	SL	Slice Coverage	Fov <sub>x</sub>	Fov <sub>y</sub>	Matrix <sub>x</sub>	Matrix <sub>y</sub>	Pixel <sub>x</sub>	Pixel <sub>y</sub>
	(T)	(s)	(#)	(ms)	(ms)	(Degrees)	(mm)	(mm)	(mm)	(mm)	(#)	(#)	(mm)	(mm)
<b>MetSyn</b>	3	21	60–72	9.1	1.2, 2.5, 3.7, 5.0, 6.2, 7.5	4	5	300–360	280–402	334–500	128–162	224–256	1.89–2.56	1.3–2.32
<b>Control</b>	1.5	22	60–72	9.1	2.4, 4.8, 7.1, 9.5, 11.9, 13.9	5	5	300–360	240–345	340–460	72–90	160–224	2.18–3.83	1.96–2.88

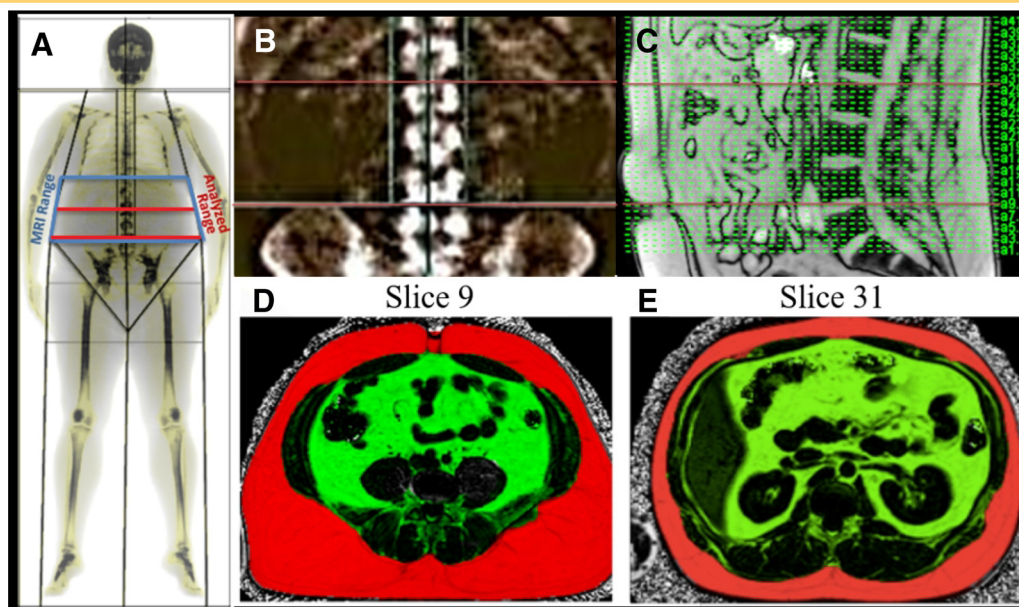


**Figure 1.** Dual-energy x-ray absorptiometry (DXA) versus magnetic resonance imaging (MRI) normalization and visceral adipose tissue (VAT) imaging procedure. DXA scan overlay with imaging ranges indicated (A), DXA scan vertebral localization (B), MRI imaging sagittal plane vertebral localization (C), lower boundary MRI slice image (D), and upper boundary MRI slice image (E). Selected images are uploaded into MATLAB with semiautomated mask generation edited for accuracy (Figure 2). Subcutaneous adipose tissue (SAT) is depicted in RED and VAT is depicted in GREEN.

the abdominal region. In step 2 (Figure 2B), the visceral mask was created by applying thresholds  $FP < 50\%$ ,  $WP > 40\%$ , and  $water > 10$  to all pixels within the previously defined abdominal region. All pixels with signal intensity  $\leq 10$  in the water image were eliminated because of their very low signals that most likely represented noise. This threshold eliminated  $\sim 0.75\%$  of those voxels within the abdomen with  $FP \leq 50\%$  and  $WP \geq 40\%$ . Morphological operations of dilation followed by erosion were then applied to close any boundary gaps. In step 3, (Figure 2C), the subcutaneous region was defined by subtracting the visceral region from the abdominal region. Finally, in step 4 (Figure 2C), the resulting visceral and subcutaneous regions were visually checked by the user and manually corrected if needed. Manual correction rates were tracked by classifying each image as requiring no correction, minor correction, or major correction. A minor correction was defined as VAT and SAT regions successfully recognized as independent regions, but requiring a small manual correction to an incorrectly identified region. A major correction was defined as an algorithm failure to identify a full fat region requiring complete manual definition.

Following visual confirmation of the pixels defined as VAT and SAT, the volume of each compartment was calculated. Any voxel with an in-phase image intensity  $\geq 40$  and  $FP \geq 50\%$  was defined as a fat voxel. The threshold on in-phase signal intensity was intended to prevent noise pixels from counting as fat. It eliminated voxels at the very low end of the signal intensity distribution representing  $< 1\%$  of all voxels in the SAT region, and  $< 2\%$  of all voxels in the VAT region. VAT and SAT volumes were calculated as the product of the number of fat voxels in each respective region, and the voxel volume (cc). VAT and SAT

volumes were multiplied by an assumed constant adipose tissue density (0.92 g/cc) (18) to convert to mass (kg). The VAT/SAT ratio was also calculated for subsequent comparison with DXA.

#### Hepatic Fat Percentage MRI Measurement

The entire liver was included within the single breath-hold VARPRO scan and the images used to measure proton density hepatic fat fraction (23–25). Fat fraction was measured in each of the 9 segments (26) of the liver by manually drawing ROIs in 3 slices defined by the anatomy. First, the hepatic portal vein (HPV) slice was defined as the slice separating the 5 superior segments from the 4 inferior segments, and the top half from bottom half of the liver. Then, the most superior and most inferior slices in which each liver segment was visible and free from significant artifact or blood vessels were identified and used for quantification.

ImageJ software (27) was used to draw circular ROIs (17.32 mm in diameter) in all segments at the most superior and inferior slices, the slice nearest the HPV, and the slice in between and equidistant to both, avoiding large blood vessels and visible image artifacts. Thus, 3 ROIs were drawn in each of the 9 liver segments. The 3 measurements in each segment were averaged over the height of the liver to measure segmental fat fraction, and then the measurements for the nine segments were averaged to provide a single liver fat fraction for each subject (28).

#### Intra- and Interobserver Reproducibility

Five subjects were randomly chosen from each of the 2 cohorts to evaluate intra- and interobserver reproducibility of the MRI VAT quantification process. A single observer quantified the images from these 10 subjects on 2 separate occasions  $\sim 8$

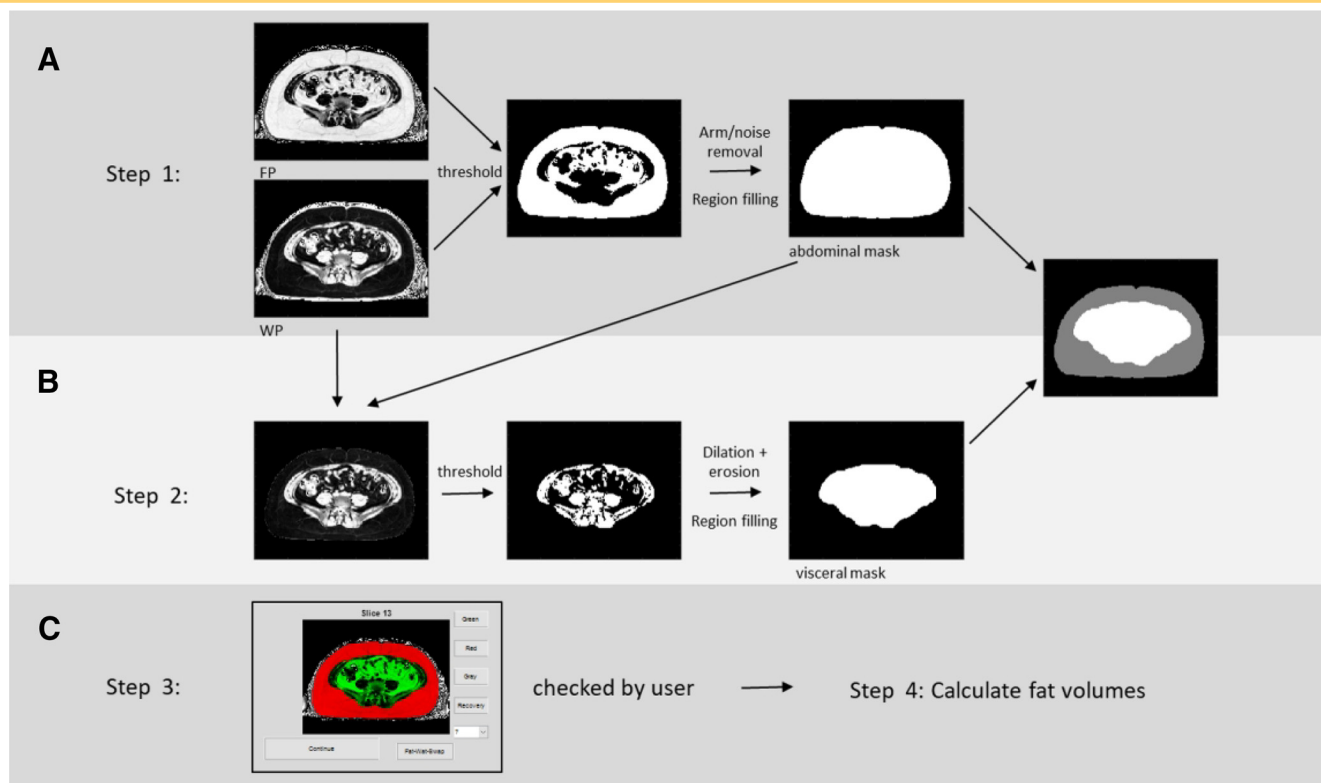


**Figure 2.** Flowchart of semiautomated MRI VAT and SAT quantification. Defining the abdominal region by thresholding fat percentage and water percentage images, following with morphological operations (A). Defining the visceral region by thresholding fat percentage, water percentage and water images within abdominal region, then following with morphological operations (B). Manual correction and fat volume calculation (C).

months apart, and 2 observers independently quantified the same data sets blinded to the results of the other observer.

**Statistical Analysis**

Continuous variables were expressed as mean ± SD. Measurements were compared using independent-sample *t* tests and univariate analysis of variance. Bland–Altman (29) analysis was used to evaluate agreement between MRI and DXA, and correlation plots were used to assess interchangeability. Two-way random intraclass correlation (ICC) was used to evaluate intraobserver repeatability and interobserver reproducibility. Statistical analysis was performed using SPSS Statistics version 24 (IBM Corp., New York, NY). Statistical significance was set ( $P < .05$ ), *a priori*.

**RESULTS**

The need for manual correction of the MRI fat quantification results differed between the MetSyn and Control groups. In the MetSyn group, 65% of the images needed no correction and 35% required a minor correction, with none requiring major correction. In the Control group, 60% of the images needed no correction, 33% required minor correction, and 7% required major correction.

Correlation and Bland–Altman plots comparing DXA and MRI across all subjects are shown in Figure 3. MRI and DXA VAT results were highly correlated and interchangeable in the

MetSyn, Control, and combined cohorts (Figure 3A), although DXA showed a slight positive bias (+0.064 kg) relative to MRI (Figure 3B). SAT results, on the other hand, were significantly different between the 2 modalities.

DXA SAT values showed a negative bias with respect to MRI in individuals with greater SAT mass (Figure 3C and Figure 3D). Although strongly correlated in the controls, the correlation between DXA and MRI SAT was surprisingly poor in MetSyn patients (Figure 3C). Consequently, DXA-derived VAT/SAT ratio (Figure 3, E and F) was significantly higher than MRI-derived value in MetSyn patients ( $P = .005$ ) and the combined group ( $P = .036$ ).

Both MRI and DXA were able to differentiate MetSyn patients from controls based on central adiposity (Figure 4). VAT and SAT measurements were significantly different between the 2 groups ( $P = .001$ ). VAT/SAT ratio quantified by MRI was approximately 43% higher in MetSyn ( $0.72 \pm 0.31$ ) than in controls ( $0.41 \pm 0.28$ ;  $P = .003$ ). VAT/SAT ratio quantified via DXA was also elevated in MetSyn ( $1.08 \pm 0.54$ ) more than in controls ( $0.53 \pm 0.35$ ;  $P = .001$ ). MRI and DXA results were compared in each of the cohorts. VAT results from MRI and DXA were not significantly different for controls or MetSyn. VAT/SAT ratio by MRI and DXA did not differ in the controls ( $P = .116$ ).

The results of reproducibility analysis of MRI VAT are provided in Table 3. Intraobserver and interobserver standard error of

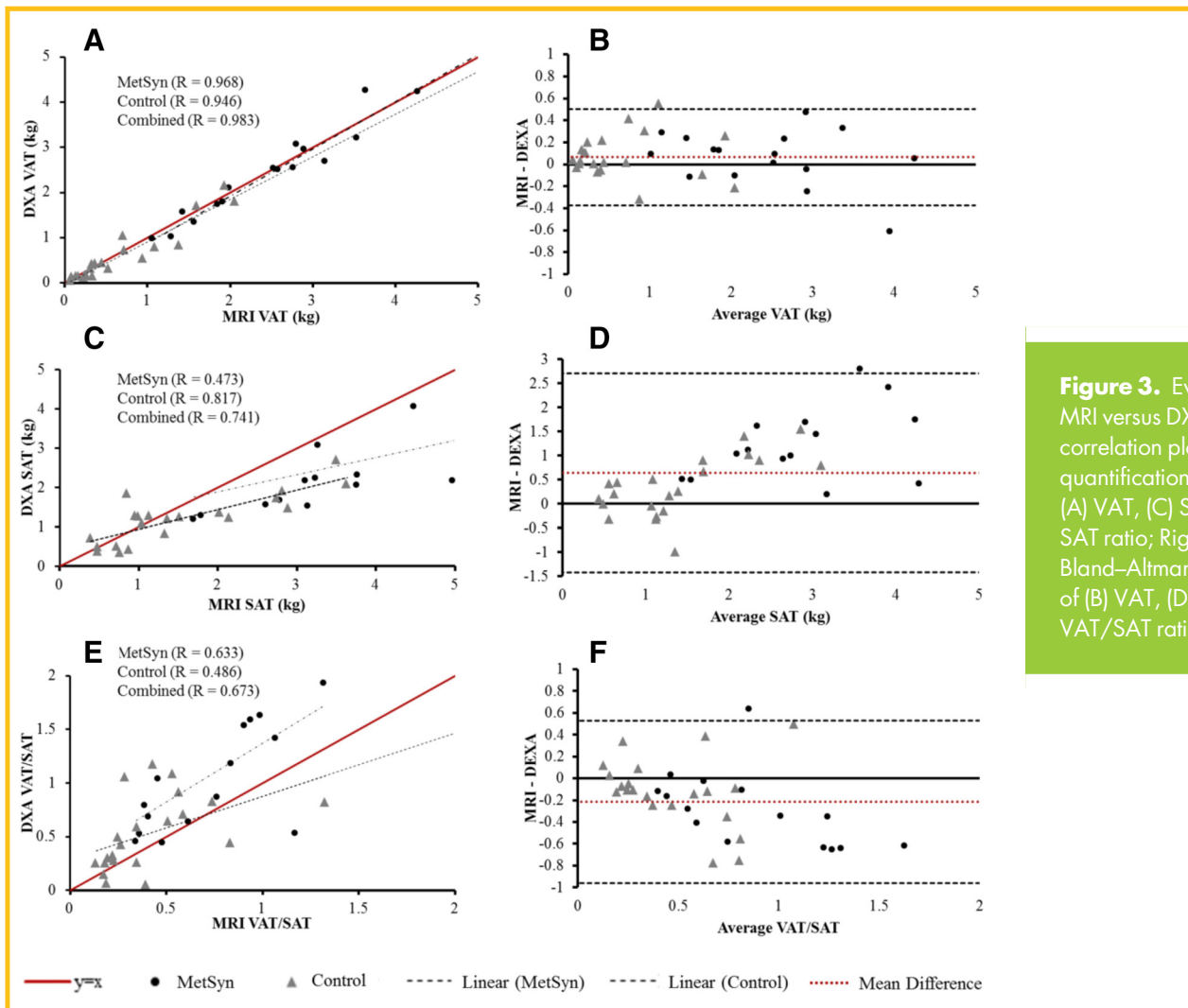


**Figure 3.** Evaluation of MRI versus DXA. Left side—correlation plots of MRI fat quantification versus DXA (A) VAT, (C) SAT, (E) VAT/SAT ratio; Right side—Bland–Altman comparisons of (B) VAT, (D) SAT, and (F) VAT/SAT ratio.

the mean was approximately 0.4 kg. Absolute intraobserver mean difference was 0.07 kg, while interobserver absolute mean difference was 0.28 kg. Mean correlation coefficient was 0.99. Intraclass correlation coefficients for both intra- and interobserver comparisons indicate excellent reliability of measures  $>0.95$  (30).

Whole-body fat percentage measured by DXA was significantly higher in MetSyn ( $42.0\% \pm 8.1\%$ ) than in Control cohort ( $26.7\% \pm 6.9\%$ ;  $P = .001$ ), and was moderately correlated ( $R = 0.575$ ) with VAT measured via MRI. Liver fat fraction measured by MRI was significantly higher ( $P = .001$ ) in MetSyn patients ( $12.4\% \pm 7.6\%$ ) than in controls ( $2.6\% \pm 2.2\%$ ). Liver fat also showed a strong positive correlation with MRI VAT ( $R = 0.778$ ). Incidental findings ranging from hepatic steatosis to abdominal cysts and degenerative changes of the spine were detected on MRI scans in 14/16 (87.5%) of the MetSyn patients but in none of the Control group; three of these findings were deemed serious enough to warrant physician follow-up.

## DISCUSSION

DXA is the most commonly used method of whole-body and abdominal fat quantification, and it has demonstrated utility in estimating VAT (7). Although more costly than DXA, the

accuracy of MRI body fat measurement is well-established (31), and aside from autopsy and cadaver studies, MRI and CT are considered as gold standards for adipose tissue quantification (16). In this study we compared DXA fat quantification with an anatomically matched, semiautomated MRI measurement of abdominal VAT and SAT. DXA measurements of VAT have been shown previously to correlate with MRI in larger multiethnic cohorts (18), and similar to the results of previous literature (17, 19), our results indicate that anatomically-matched ROIs produce VAT measurements that are not only correlated but also interchangeable. This concordance was maintained across subjects with a wide range of VAT mass ranging from  $<1$  kg to  $\sim 4.5$  kg.

There was, however, a significant difference between the two modalities in computed VAT/SAT ratios in the MetSyn cohort. Considering MRI as the reference standard, DXA underestimated SAT and therefore overestimated VAT/SAT ratio relative to MRI in subjects with high SAT. Careful review of the MRI images revealed 2 MetSyn cases in which SAT may have been slightly *underestimated* by MRI. In 1 participant, a small amount of SAT appeared to lie outside of the image FOV and was therefore unaccounted for; in another case, the fat–water separation algorithm failed, obscuring a portion of SAT in only a subset of

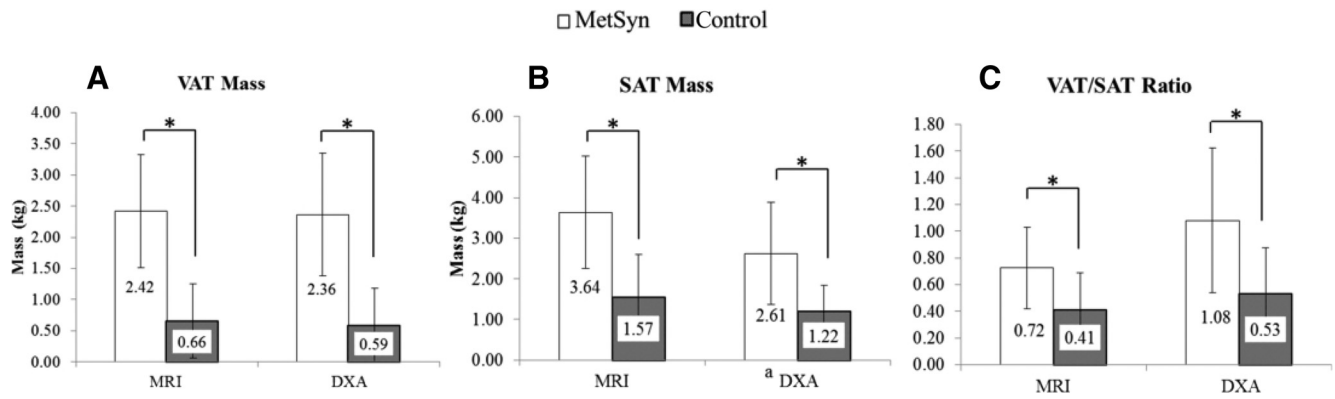


**Figure 4.** MRI and DXA measures of central adiposity. Data are shown as mean ± SD. VAT Mass (A), SAT Mass (B), VAT/SAT Ratio (C).

\*Statistical significance between groups,  $P < .05$  Equations and conversions:  $^a(cc \times 0.92)/1000 = \text{mass (kg)}$ .

slices in 1 subject. In both of these cases, however, the observed error would have led to an underestimation of SAT by MRI, and therefore, it did not contribute to the observed relative underestimation of SAT by DXA, which was perhaps due to the lack of uniformity in the layer thickness within the SAT depot. Previous research suggests that variability in SAT thickness is dependent upon anatomical location (32), illustrating the need for cross-sectional imaging for precise quantification of SAT. The relative distribution of fat expressed as VAT/SAT ratio has been shown to be related to increased cardiometabolic risk independent of total VAT or BMI (5). Kaess et al. (33) found that high VAT/SAT ratio is associated with MetSyn risk factors including low HDL concentration, high triglyceride concentration, and hypertension, when adjusted for total VAT. Our results suggest that DXA may be less accurate for SAT measurement in subjects with higher fat burden, and this should be considered when VAT/SAT ratio is of interest.

All major corrections were required in the Control group and none in the MetSyn group; these were caused by failure of the algorithm to detect the SAT layer in thinner Control subjects. Despite the use of manual corrections, the MRI VAT measurements demonstrated excellent intra- and interobserver reproducibility. The average difference between intraobserver measurements was <0.1 kg, or <6%. The average interobserver difference was over 3-fold higher, indicating that training and familiarization may be

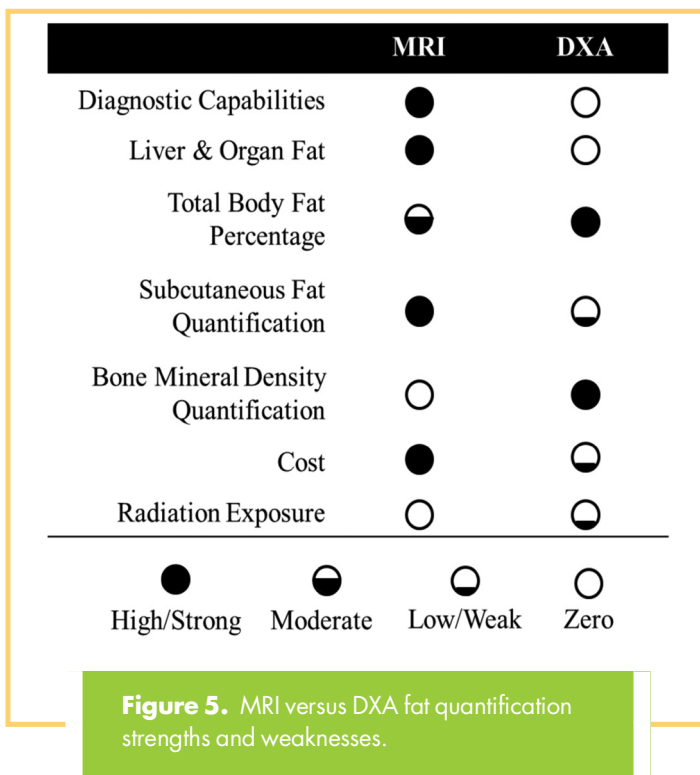
important for consistency between technicians. Further investigation revealed that differences in the MRI slices included in the analysis by the 2 observers played a significant role in this variability. When matched such that the 2 observers analyzed the same number of slices, the percent difference dropped to approximately the intraobserver level (4.9%). Reproducibility was not measured for the DXA scans, which were performed only once and were automatically analyzed without operator interaction.

In a single breath-hold MRI scan, abdominal SAT, VAT, and liver fat fraction can all be quantified. DXA, on the other hand, is incapable of organ tissue fat fraction measurement. It has been previously shown that visceral fat deposition is directly correlated with liver inflammation and fibrosis and presents a central target for future interventions in nonalcoholic fatty liver disease (NAFLD) (34). Elevated liver fat is also associated with increased risk of metabolic disease (35, 36), cardiovascular disease (3, 37), and certain cancers (37). In our study cohort, participants with MetSyn were found to have, on average, a 6-fold higher liver fat percentage than Control participants and a strong positive correlation was found between liver fat fraction and VAT in the combined cohort.

DXA and MRI each have inherent advantages and disadvantages that may favor the use of one over the other depending on the application in research or clinical patient assessment (Figure

**Table 3.** MRI VAT Quantification Repeatability and Reproducibility

	MRI Intraobserver (CC)		MRI Interobserver	
	Measure 1	Measure 2	Observer 1 (CC)	Observer 2 (RL)
Sample Size	10	10	10	10
VAT Mean (kg)	1.59	1.60	1.59	1.60
Standard Error of the Mean (kg)	0.40	0.42	0.40	0.40
Absolute Mean Difference (kg)	0.07		0.28	
Mean Percent Difference (%)	5.71		20.16	
ICC	0.998		0.977	



5). Although MRI has enhanced diagnostic and organ fat capabilities, DXA is relatively low cost even when not covered by a third party or insurance. DXA imaging is increasingly used for body composition assessment in fitness centers, amateur and professional athletics, and some clinical scenarios (35-37). DXA also provides bone mineral density information, although it exposes individuals to very-low-level radiation, similar to the amount one might experience during a cross-country flight (38). DXA can provide a rapid, automated assessment of whole-body and visceral fat, but in our study, was less accurate for SAT and VAT/SAT ratio. MRI fat quantification is better suited as an adjunct to clinical abdominal MRI examinations in patient populations in whom the breadth of diagnostic information provided can be helpful for directing therapy; this was evidenced by the high rate of incidental findings in the MetSyn cohort. The single breath-hold VARPRO scan used in our study to measure VAT, SAT, and liver fat fraction takes about 20 seconds and is easily incorporated into a comprehensive abdominal imaging exam. Although DXA was shown in our study to provide an accurate assessment of VAT that matched MRI results, DXA does not provide the breadth of clinical information afforded by MRI.

### Limitations

The data used for this study came from 2 separate trials; the MetSyn patients were scanned on a 3 T system and the controls

### ACKNOWLEDGMENTS

OPS receives research funding support from The Robert F. Wolfe and Edgar T. Wolfe Foundation and from Siemens Healthineers.

on a 1.5 T system. The bore sizes were the same for these 2 systems (60 cm in diameter), and the fat-water separation techniques were equivalent; however, it is known that B0 and B1 field inhomogeneity is greater at a higher field. Although the use of intensity-based thresholds could have made the quantification algorithm sensitive to signal inhomogeneity, a review of the images and segmentation results showed no evidence of this, and a manual correction process was employed to minimize errors.

A single estimated adipose tissue density (0.92 g/cc) (18) was used to compute fat mass from volume regardless of the fat depot; however, VAT and SAT density may differ owing to factors such as blood flow, endocrine function, and lipid turnover rate (38), and this may also vary between individuals (39). This variability may have introduced some error in converting fat volume to mass.

The term “VAT” as used in this study for both MRI and DXA measurements, and as commonly used in the literature, liberally included all abdominal fat that is not subcutaneous fat; however, this definition more accurately applies to IAAT (13, 14). Although VAT is the largest component, IAAT also includes spinal, intraorgan, retroperitoneal, and intramuscular fat (13), which have distinct physiological relevance. For example, it has been suggested that retroperitoneal fat has hormonal effects (40) and affects cardiometabolic health in humans (41). DXA is based on 2-dimensional projection data (9) and has no potential to analyze the separate subcomponents of IAAT. MRI, on the other hand, offers the possibility of accurately subsectioning IAAT further to arrive at a true VAT measurement, although currently, this would require painstaking manual segmentation. It is not yet clear whether such further subclassification of IAAT subcomponents would be clinically relevant (42) or provide reliable, independent predictive information related to metabolic and cardiovascular disease risk.

DXA reproducibility was not analyzed. The software is nearly fully automatic and has been previously shown to be highly reproducible (43); therefore, we felt that additional measurement and associated radiation exposure to measure DXA reproducibility was not warranted.

This study compared DXA and MRI VAT and VAT/SAT ratio measured within an anatomically matched field of view in a cohort including Control subjects and MetSyn patients exhibiting a wide range of VAT volume. Our results showed VAT measured by DXA and MRI to be interchangeable, while VAT/SAT ratio measurements differed between the 2 modalities. DXA can play an important role in basic body composition analysis and may be used to assess responses to diet, training, and therapeutic interventions. Quantification of abdominal adipose tissue depots by MRI, on the other hand, can be easily incorporated into clinical imaging protocols in patients indicated for abdominal MRI and can simultaneously provide important assessment of liver fat fraction.

**REFERENCES**

1. Schäffler A, Schölmerich J, Büchler C. Mechanisms of disease: adipocytokines and visceral adipose tissue—emerging role in nonalcoholic fatty liver disease. *Nat Rev Gastroenterol Hepatol.* 2005;2:273.
2. Borga M, West J, Bell JD, Harvey NC, Romu T, Heymsfield SB, Dahlqvist Leinhard O. Advanced body composition assessment: from body mass index to body composition profiling. *J Investig Med.* 2018;66:1–9.
3. Després JP. Body fat distribution and risk of cardiovascular disease: an update. *Circulation.* 2012;126:1301–1313.
4. Kwon H, Kim D, Kim JS. Body fat distribution and the risk of incident metabolic syndrome: a longitudinal cohort study. *Sci Rep.* 2017;7:10955.
5. Ladeiras-Lopes R, Sampaio F, Bettencourt N, Fontes-Carvalho R, Ferreira N, Leite-Moreira A, Gama V. The ratio between visceral and subcutaneous abdominal fat assessed by computed tomography is an independent predictor of mortality and cardiac events. *Rev Esp Cardiol (Engl Ed).* 2017;70:331–337.
6. Kaul S, Rothney MP, Peters DM, Wacker WK, Davis CE, Shapiro MD, Ergun DL. Dual-energy X-ray absorptiometry for quantification of visceral fat. *Obesity.* 2012;20:1313–1318.
7. Mohammad A, De Lucia Rolfe E, Sleigh A, Kivisild T, Behbehani K, Wareham NJ, Brage S, Mohammad T. Validity of visceral adiposity estimates from DXA against MRI in Kuwaiti men and women. *Nutr Diabetes.* 2017;7:e238.
8. Bazzocchi A, Diano D, Ponti F, Salizzoni E, Albinetti U, Marchesini G, Battista G. A 360-degree overview of body composition in healthy people: relationships among anthropometry, ultrasonography, and dual-energy x-ray absorptiometry. *Nutrition.* 2014;30:696–701.
9. Bazzocchi A, Ponti F, Albinetti U, Battista G, Guglielmi G. DXA: technical aspects and application. *Eur J Radiol.* 2016;85:1481–1492.
10. Graffy PM, Pickhardt PJ. Quantification of hepatic and visceral fat by CT and MR imaging: relevance to the obesity epidemic, metabolic syndrome and NAFLD. *Br J Radiol.* 2016;89:20151024.
11. Hu HH, Li Y, Nagy TR, Goran MI, Nayak KS. Quantification of absolute fat mass by magnetic resonance imaging: a validation study against chemical analysis. *Int J Body Compos Res.* 2011;9:111–122.
12. Hu HH, Nayak KS, Goran MI. Assessment of abdominal adipose tissue and organ fat content by magnetic resonance imaging. *Obes Rev.* 2011;12:e504–e15.
13. Staiano A, Katzmarzyk P. Ethnic and sex differences in body fat and visceral and subcutaneous adiposity in children and adolescents. *Int J Obes.* 2012;36:1261.
14. Shen W, Wang Z, Punyanita M, Lei J, Sinav A, Kral JG, Imielinska C, Ross R, Heymsfield SB. Adipose tissue quantification by imaging methods: a proposed classification. *Obes Res.* 2003;11:5–16.
15. Nishimura H, Zhang Y, Ohkuma K, Uchida M, Hayabuchi N, Sun S. MR imaging of soft-tissue masses of the extraperitoneal spaces. *Radiographics.* 2001;21:1141–1154.
16. van der Kooy K, Seidell JC. Techniques for the measurement of visceral fat: a practical guide. *Int J Obes Relat Metab Disord.* 1993;17:187–196.
17. Silver HJ, Niswender KD, Kullberg J, Berglund J, Johansson L, Bruvold M, Avison MJ, Welch EB. Comparison of gross body fat-water magnetic resonance imaging at 3 Tesla to dual-energy X-ray absorptiometry in obese women. *Obesity.* 2013;21:765–774.
18. Neeland IJ, Grundy SM, Li X, Adams-Huet B, Vega GL. Comparison of visceral fat mass measurement by dual-X-ray absorptiometry and magnetic resonance imaging in a multiethnic cohort: the Dallas Heart Study. *Nutr Diabetes.* 2016;6:e221–e.
19. McCauley LS, Ghatas MP, Sumrell RM, Cirnigliaro CM, Kirshblum SC, Bauman WA, Gorgey AS. Measurement of visceral adipose tissue in persons with spinal cord injury by magnetic resonance imaging and dual X-ray absorptiometry: generation and application of a predictive equation. *J Clin Densitom.* 2018.
20. Alberti KGMM, Eckel RH, Grundy SM, Zimmet PZ, Cleeman JI, Donato KA, Fruchart J-C, James WPT, Loria CM, Smith SC, International Diabetes Federation Task Force on Epidemiology and Prevention; National Heart, Lung, and Blood Institute; American Heart Association; World Heart Federation; International Atherosclerosis Society; International Association for the Study of Obesity. Harmonizing the metabolic syndrome: a joint interim statement of the International Diabetes Federation Task Force on Epidemiology and Prevention; National Heart, Lung, and Blood Institute; American Heart Association; World Heart Federation; International Atherosclerosis Society; and International Association for the Study of Obesity. *Circulation.* 2009;120:1640–1645.
21. Hutton C, Gyngell ML, Milanese M, Bagur A, Brady M. Validation of a standardized MRI method for liver fat and T2\* quantification. *PLoS One.* 2018;13:e0204175.
22. Hernandez D, Haldar JP, Sutton BP, Ma J, Kellman P, Liang Z-P. Joint estimation of water/fat images and field inhomogeneity map. *Magn Reson Med.* 2008;59:571–580.
23. Patel N, Peterson M, Brenner D, Heba E, Sirlin C, Loomba R. Association between novel MRI-estimated pancreatic fat and liver histology-determined steatosis and fibrosis in non-alcoholic fatty liver disease. *Aliment Pharmacol Ther.* 2013;37:630–639.
24. Patel NS, Doycheva I, Peterson MR, Hooker J, Kisselva T, Schnabl B, Seki E, Sirlin CB, Loomba R. Effect of weight loss on magnetic resonance imaging estimation of liver fat and volume in patients with nonalcoholic steatohepatitis. *Clin Gastroenterol Hepatol.* 2015;13:561–568.e1.
25. Sofue K, Mileto A, Dale BM, Zhong X, Bashir MR. Interexamination repeatability and spatial heterogeneity of liver iron and fat quantification using MRI-based multistep adaptive fitting algorithm. *J Magn Reson Imaging.* 2015;42:1281–1290.
26. Bonekamp S, Tang A, Mashhood A, Wolfson T, Changchien C, Middleton MS, Clark L, Gamst A, Loomba R, Sirlin CB. Spatial distribution of MRI-determined hepatic proton density fat fraction in adults with nonalcoholic fatty liver disease. *J Magn Reson Imaging.* 2014;39:1525–1532.
27. Schneider CA, Rasband WS, Eliceiri KW. NIH Image to ImageJ: 25 years of image analysis. *Nat Methods.* 2012;9:671–675.
28. Idilman IS, Anikar H, Idilman R, Kabacam G, Savas B, Elhan A, Celik A, Bahar K, Karcaalincaba M. Hepatic steatosis: quantification by proton density fat fraction with MR imaging versus liver biopsy. *Radiology.* 2013;267:767–775.
29. Martin Bland J, Altman D. Statistical methods for assessing agreement between two methods of clinical measurement. *Lancet.* 1986;327:307–310.
30. Koo TK, Li MY. A guideline of selecting and reporting intraclass correlation coefficients for reliability research. *J Chiropr Med.* 2016;15:155–163.
31. Staten M, Totty W, Kohrt W. Measurement of fat distribution by magnetic resonance imaging. *Invest Radiol.* 1989;24:345–349.
32. Lee S, Janssen I, Ross R. Interindividual variation in abdominal subcutaneous and visceral adipose tissue: influence of measurement site. *J Appl Physiol.* 2004;97:948–954.
33. Kaess BM, Pedley A, Massaro JM, Murabito J, Hoffmann U, Fox CS. The ratio of visceral to subcutaneous fat, a metric of body fat distribution, is a unique correlate of cardiometabolic risk. *Diabetologia.* 2012;55:2622–2630.
34. van der Poorten D, Milner KL, Hui J, Hodge A, Trenell MI, Kench JG, London R, Peduto T, Chisholm DJ, George J. Visceral fat: a key mediator of steatohepatitis in metabolic liver disease. *Hepatology.* 2008;48:449–457.
35. Després JP. Is visceral obesity the cause of the metabolic syndrome? *Ann Med.* 2006;38:52–63.
36. Tarantino G, Finelli C. What about non-alcoholic fatty liver disease as a new criterion to define metabolic syndrome? *World J Gastroenterol.* 2013;19:3375.
37. Sanna C, Rosso C, Marietti M, Bugianesi E. Non-alcoholic fatty liver disease and extra-hepatic cancers. *Int J Mol Sci.* 2016;17:717.
38. Rosenquist KJ, Pedley A, Massaro JM, Theriksen KE, Murabito JM, Hoffmann U, Fox CS. Visceral and subcutaneous fat quality and cardiometabolic risk. *JACC Cardiovasc Imaging.* 2013;6:762–771.
39. Martin AD, Daniel MZ, Drinkwater DT, Clarys JP. Adipose tissue density, estimated adipose lipid fraction and whole body adiposity in male cadavers. *Int J Obes Relat Metab Disord.* 1994;18:79–83.
40. Bjørndal B, Burri L, Staalesen V, Skorve J, Berge RK. Different adipose depots: their role in the development of metabolic syndrome and mitochondrial response to hypolipidemic agents. *J Obes.* 2011;2011.
41. Hung CS, Lee JK, Yang CY, Hsieh HR, Ma WY, Lin MS, Liu PH, Shih SR, Liou JM, Chuang LM, Chen MF, Lin JW, Wei JN, Li HY. Measurement of visceral fat: should we include retroperitoneal fat? *PLoS One.* 2014;9:e112355.
42. Carr DB, Utzschneider KM, Hull RL, Kodama K, Retzlaff BM, Brunzell JD, Shofer JB, Fish BE, Knopp RH, Kahn SE. Intra-abdominal fat is a major determinant of the National Cholesterol Education Program Adult Treatment Panel III criteria for the metabolic syndrome. *Diabetes.* 2004;53:2087–2094.
43. Moreira OC, Oliveira CEP, De-Paz JA. Dual energy X-ray absorptiometry (DXA) reliability and intraobserver reproducibility for segmental body composition measuring. *Nutr Hosp.* 2018;35:340–345.